ACC JOURNAL
XXVII
1/2021

Issue A

Natural Sciences and Technology

Indexed in:

Liberec – Zittau/Görlitz – Wrocław/Jelenia Góra

ACC JOURNAL je mezinárodní vědecký časopis, jehož vydavatelem je Technická univerzita v Liberci. Na jeho tvorbě se podílí čtyři vysoké školy sdružené v Akademickém koordinačním středisku v Euroregionu Nisa (ACC). Ročně vycházejí zpravidla tři čísla.

ACC JOURNAL je periodikum publikující původní recenzované vědecké práce, vědecké studie, příspěvky ke konferencím a výzkumným projektům. První číslo obsahuje příspěvky zaměřené na oblast přírodních věd a techniky, druhé číslo je zaměřeno na oblast ekonomie, třetí číslo pojednává o tématech ze společenských věd. ACC JOURNAL má charakter recenzovaného časopisu. Jeho vydání navazuje na sborník „Vědecká pojednání", který vycházel v letech 1995-2008.

ACC JOURNAL is an international scientific journal. It is published by the Technical University of Liberec. Four universities united in the Academic Coordination Centre in the Euroregion Nisa participate in its production. There are usually three issues of the journal annually.

ACC JOURNAL is a periodical publishing original reviewed scientific papers, scientific studies, papers presented at conferences, and findings of research projects. The first issue focuses on natural sciences and technology, the second issue deals with the science of economics, and the third issue contains findings from the area of social sciences. ACC JOURNAL is a reviewed one. It is building upon the tradition of the "Scientific Treatises" published between 1995 and 2008.

Contents

Research Articles

Research Articles

THE INFLUENCE OF DIFFERENT INFILL STRUCTURES ON THE MECHANICAL PROPERTIES IN ADDITIVE MANUFACTURING

Wolfgang Förster[1]; **Thomas Pucklitzsch**[2]; **Daniela Nickel**[3]

Berufsakademie Sachsen, Staatliche Studienakademie Glauchau, Industrielle Produktion,
Kopernikusstraße 51, 08371 Glauchau, Germany
e-mail: [1]wolfgang.foerster@ba-sachsen.de; [2]thomas.pucklitzsch@ba-sachsen.de;
[3]daniela.nickel@ba-sachsen.de

Abstract

Besides the outer shell, it is the internal structures that contribute the most to the mechanical integrity of an additively manufactured component. In order to investigate the influence of the geometrically different internal structures and infill density on the Young's modulus, tensile strength and failure strain, tensile specimens of polylactic Acid (PLA) were prepared using fused deposition modeling and tested at room temperature. There was a significant influence of the infill density, the manufacturing process and the resulting microstructure on the mechanical properties. In summary, the position of the microstructure relative to the load direction is found to be a significant factor of influence.

Keywords

Fused deposition modeling; PLA; Infill; Tensile test; Mechanical properties; Microstructure.

Introduction

Nature follows the principle of "as much as necessary, as little as possible". This approach ensures optimum properties while being energy- and resource-efficient at the same time. It is therefore hardly surprising that engineers try to transfer this principle to the world of technology. Components are to be as light as possible and still have excellent mechanical properties. Bones are a good example of how this works in nature. They consist of a shell, which provides a functional surface, and an internal structure, which is porous in design. Additive manufacturing can be used to artificially produce such complex components and (internal) structures. A widely used technique is the fused deposition modeling (FDM). Due to its simple design and robust functionality, it is frequently used in the field of plastics. As the print head moves, a plastic wire (filament) is conveyed from a roll to the print head, where it is melted and extruded through a nozzle. This procedure was also used for the present study. Since the internal structures determine both the mechanical integrity and the weight of the component, they offer potential for optimization. A variety of different internal structures is available for this purpose. However, which structures are suitable, and how can they be created? How do they affect the mechanical properties? Is there an optimum?

These and similar questions have already been investigated by researchers. Corresponding analyses have investigated the influence of manufacturing parameters such as layer thickness, infill density or infill structures on the mechanical properties. They included tensile tests with samples made of polylactide Acid (PLA). Low layer thicknesses resulted in higher tensile and flexural strengths while higher layer thicknesses raise both the Young's modulus and the ductility [1, 2]. Higher infill density also increases tensile strength and stiffness [3, 4, 5, 6]. The influence of the infill structures, on the other hand, can be considered minor [7, 8]. Further production parameters such as direction of production, layer thickness, printing

temperature and filament feed rate only have a slight mutual impact and therefore cannot be separated from each other [9, 1, 3, 10].

1   Research Subject

Previously published studies show an effect on mechanical properties; however, they lack a rationale for their observations. Our investigations are intended to provide information about possible causes. To ensure comparability, we are also using tensile tests with samples made of PLA as well as fused deposition modeling as an additive manufacturing process.

2   Experimental Investigations

2.1   Specimens Preparation

Tensile testing was used to provide easy access to the measurement of the mechanical properties. For this purpose, flat tensile specimens of shape 1B according to DIN EN ISO 527-2 were used, which has the advantage that the specimens can be reproducibly fabricated using fused deposition modeling. In addition, tensile stresses are significant contributors to component failures.
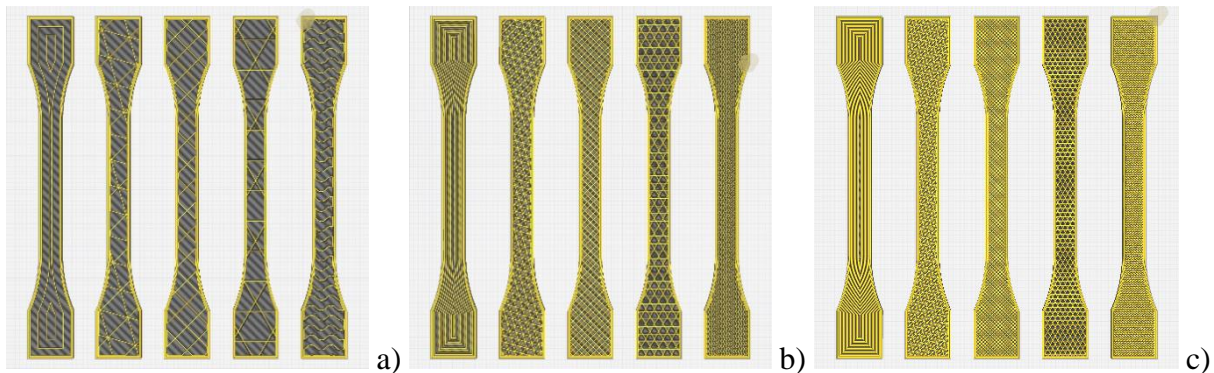
Source: Own work

Fig. 1:   *Sectional view of the used flat tensile specimens in the slicer software CURA for an infill density of a) 10%, b) 40% and c) 70%. The structures used, in each case from left to right: concentric, triangles, grid, cubic subdivision and gyroid*

In order to investigate whether and how the mechanical properties are influenced by different infill structures, the slicer software CURA was used to select five infill structures which differ from each other to as great an extent as possible. The slicer is an important and necessary tool in the field of additive manufacturing. It breaks down the digital model of the object to be produced into individual layers. This information is then passed on to the 3D printer and scanned by the print head. The slicer also calculates the most efficient way to deposit the print material in the right positions within a layer. All print parameters and infill structures can be adjusted here. This produces the layered structure characteristic of additive manufacturing. The selected infill structures range from simple lines to 2D structures and more complex three-dimensional structures. Since the interaction between the shell and the infill structure is always decisive for mechanical stability of an additively manufactured component, the tensile specimens are also coated with a shell of 1 mm thickness. In addition to the structures, their infill densities were also varied. The infill density is the percentage to which the specimen volume is filled with material. This ranged from 0% – i.e. hollow specimens – to a 10%, 40%, 70% and 100% infill. Figure 1 shows the sectional view of the tensile specimens with the infill structures used and an infill density of 40% in the slicer software.

For statistical validation, each configuration included at least three tests. The specimens were fabricated by fused deposition modeling on a commercial ULTIMAKER S5 3D printer, with five specimens fabricated at a time as shown in Figure 1. Table 1 summarizes important manufacturing parameters. A standard polylactide Acid filament from the manufacturer FormFutura was used as a material.

Tab. 1: Overview of used manufacturing parameters, infill densities and infill structures.

| Infill Pattern	Gyroid, Concentric, Triangles, Grid, Cubic Subdivision
Infill Density	0%, 10%, 40%, 70%, 100%
Nozzle Diameter	0.4 mm
Print Temperature	200 °C
Print Speed	50 mm/s
Layer Height	0.1 mm
Wall Thickness	1 mm
Line Width	0.3 mm

Source: Own

2.2   Experimental Procedure

The tensile tests were performed in-house on a TIRA 28100 tension/compression testing machine at room temperature. Prior to the test, the tensile specimens were stored for at least 24 hours in a climatic cabinet at constant temperature and humidity and only removed, weighed and clamped in the testing machine immediately before the start of the test. The tests were load-controlled at a traverse speed of 1 mm/min. To ensure the most accurate determination of the Young's modulus, the displacement was measured with an extensometer at the beginning of the test and removed again at 5% strain upon indication by the testing software. The test was terminated either when the specimen broke or when the force dropped to 80% of the maximum load.

3   Results and Discussion

3.1   Correction Factor
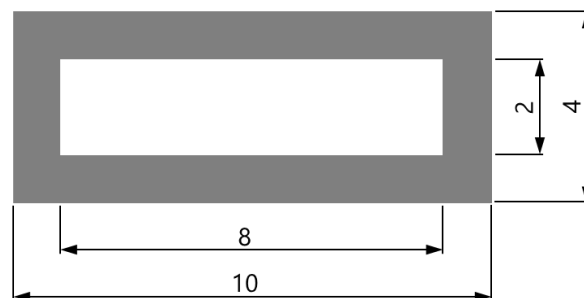
Source: Own

Fig. 2: Schematic view of the cross-section of a hollow specimen with the corresponding dimensions

The force and displacement data measured in the tensile tests are used to calculate the requested parameters such as the Young's modulus or tensile strength. In the classic tensile test, the cross-sectional area of the tested specimens is also significant as it influences the

magnitude of the occurring stresses. A homogeneous area is assumed, which would correspond to a rectangle of a 10x4 mm2 area as shown in Figure 2.

In this test, however, the infill densities were specifically varied, which results in a reduced underlying cross-sectional area as a function of the infill density. This circumstance must also be considered when calculating the mechanical parameters. For this purpose, a correction factor $m_{specific}$ in dependence of the specimen mass was used since the weight equally drops with decreasing infill densities. Thus, the correction factor is calculated from the ratio of the specimen mass with an infill density lower than 100% to the mass of specimens with a 100% infill density. For a hollow specimen, as shown in Figure 2, the correction factor is calculated to be 0.6, which means that the weight of the hollow specimen is approximately 60% of the weight of a solid specimen.

(weight of solid specimen) $m_0 = 10,5111\ g$ (1)

(weight of hollow specimen) $m = 6,4085\ g$ (2)

$$m_{specific} = \frac{g}{g_0} = \frac{6,4085\ g}{10,5111\ g} = 0,6097 \triangleq \underline{\underline{60\%}}$$ (3)

The accuracy of this assumption is shown by comparison with the percentage of the remaining cross-section for the hollow specimen. Correspondingly, it amounts to 60% of the cross-sectional area of a solid specimen.

(area of frame) $A_{frame} = 10\ mm \cdot 4\ mm - 8\ mm \cdot 2\ mm = \underline{\underline{24\ mm^2}}$ (4)

$$Proportion_{frame} = \frac{24\ mm^2}{10\ mm \cdot 4\ mm} = 0,6 \triangleq \underline{\underline{60\%}}$$ (5)

To calculate the (specific) mechanical properties depending on the infill density, the Young's modulus and tensile strength were multiplied by the correction factor $m_{specific}$ as both parameters are directly dependent on the cross-sectional area. For a qualitative classification, the results are compared with the values from the manufacturer's data sheet.

3.2   Mechanical Properties

Figure 3 shows the diagrams containing the average values for the Young's modulus, tensile strength and failure strain.

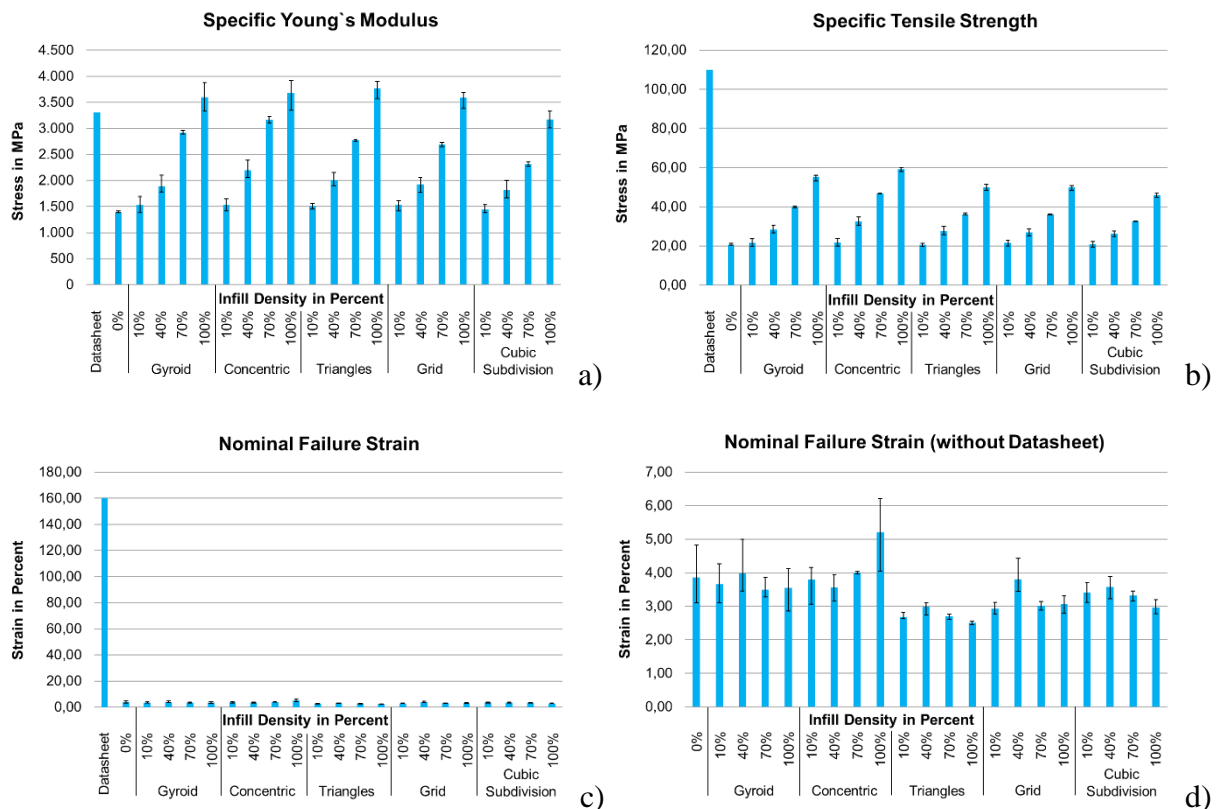### 3.2.1   Specific Young's Modulus

The Young's modulus is a material parameter that characterizes the resistance to reversible deformation. It is a measure of a material's stiffness.

As expected, the lowest value for the Young's modulus is obtained for the hollow specimen, i.e. with a 0% infill density. The values for the Young's modulus rise linearly with increasing infill densities. This behavior can be observed in all the infill structures under investigation. A closer examination of the identical infill densities of the different structures shows that the differences become more pronounced as the infill density increases. At an infill density of 10%, the values are almost equal; at 40% and 70%, the values are noticeably higher, especially for the concentric structure.

In comparison with the manufacturer's data sheet for the PLA used, the values of the specimens with a 100% infill density are slightly above the specified values. However, the higher dispersion must also be considered here. Furthermore, the values are only comparable

to a limited extent since the specifications from the data sheet refer to injection-molded specimens. These have a homogeneous microstructure in contrast to the additively manufactured specimens, which exhibit an inhomogeneous microstructure resulting from the layered structure.

In addition, the Young's modulus is by definition a characteristic material parameter that is determined on homogeneous (pore-free) specimens. If, due to pores or other structures, the microstructure deviates from this state, the Young's modulus becomes structure-dependent. It thus rather constitutes a parameter of the overall structure than that of the material. Therefore, only the values for the specimens with a 100% infill density are comparable.

Source: Own

Fig. 3: *Result diagrams of the mean values for a) specific Young's modulus, b) specific tensile strength, c) nominal failure strain with data sheet values and d) nominal failure strain without data sheet values*

3.2.2 Specific Tensile Strength

The tensile strength indicates the maximum load that can be applied to the specimen before it starts to fail.

The tensile strength values show results similar to those for the Young's modulus. There is also a linear rise with an increasing infill density, as well as differences at the same infill density with a better performance of the concentric structure.

Compared to the values of the data sheet, however, the test results are significantly lower and reach only about 50%.

3.2.3 Nominal Failure Strain

Failure strain characterizes the deformation capacity of a material until failure due to fracture, which is also referred to as ductility.

The difference to the data sheet becomes particularly obvious in respect of the failure strain values. According to the manufacturer, the homogeneous microstructure of the injection-molded specimen achieved a failure strain of 160%. In contrast, the investigations presented here only resulted in values between 2% and 4%! They are, however, not uncommon and remain within the range of values also found in literature [11, 12]. This also applies to the values of the Young's modulus and tensile strength. For the investigated structures, no tendency with increasing infill density can be detected for fracture strain. The values rather seem to be independent of the infill density and are at a specific level for the respective structures. Only for the concentric structure, the failure strain also increases with higher infill rates. However, the data vary widely around their mean value, which can lead to misinterpretation. This is caused by production-related variations in the quality of specimens.

4   Discussion

The results observed in this examination reveal three influencing factors that determine the mechanical properties.

For both the Young's modulus and the tensile strength, a linear growth of the values could be observed with an increasing infill density. This applies to all the structures studied. The rising infill density also leads to an increase in the load-bearing cross-section of the specimens, which means that more load is required for deformation. Thus, if the infill density reaches 100%, values that are comparable with the data sheet are achieved.

The manufacturing process used determines the resulting microstructure in the specimen. The microstructure is, in turn, the main parameter that influences the mechanical properties. Figure 4 shows the fracture points of a specimen with 40% concentric (a) and 40% grid structure (b).
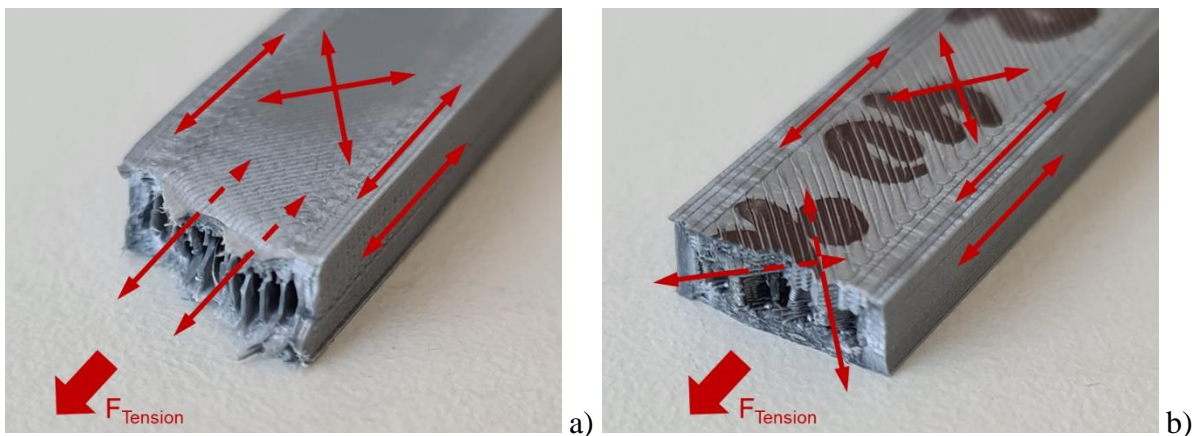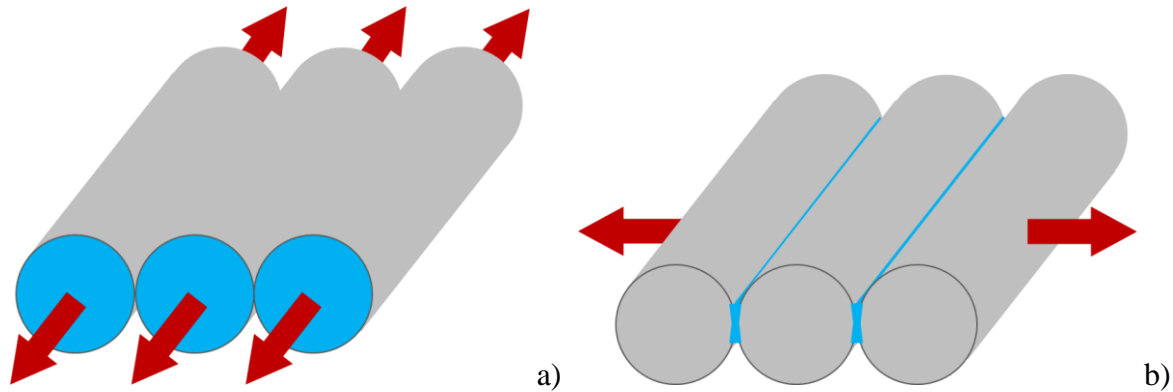

Source: Own

Fig. 4:   *Images of the fracture faces of a tensile specimen with a) 40% concentric structure and b) 40% grid structure*

Due to the path of the print head during manufacture, different deposition directions of the filament line occur within the component. In the concentric structure, all the constituents are arranged in the tensile direction of the specimen, as are the lateral faces of the specimen. Only the top and bottom faces show a 45° angle to the tensile direction. Here, the majority of the filament lines are loaded in their deposition direction and over the entire cross-sectional area (see Figure 5a). This results in significantly higher values for the Young's modulus and tensile strength, which is also reported by other authors [7]. In the specimen with grid structure, only the side faces are arranged in the tensile direction of the specimens. The infill structure as well as the top and bottom faces are at a 45° angle to the tensile direction. In this

case, only a small part of the filament lines is loaded in the deposition direction, however, most of them at an angle of 45°. This has an impact on the load-bearing cross-section of the specimens since it is reduced to the contact areas between the individual filament lines, as illustrated in Figure 5b. The better performance of the concentric structure is therefore related to the position of the filament lines in the direction of loading. The lower values for tensile strength are likewise due to the existing microstructure. Even when favorably positioned with respect to the loading direction, the inhomogeneity caused by the layered structure reaches only 50% of the values of a homogeneous specimen.

Source: Own

Fig. 5: *Schematic representation of a) loading in the direction of deposition and b) at an angle up to 90° to the direction of deposition*

The behavior of the fracture strain can also be attributed to the prevailing microstructure. Due to the inhomogeneity compared to the injection molded specimens, only a fraction of the values indicated in the data sheet are achieved. As it can be seen in the macro images of the fracture faces in Figure 6a, the favorable position with respect to the loading direction also increases the deformability of the specimen, resulting in ductile fracture, which is well visible in the fibrous structure of the fracture face. The unfavorable position of the filament lines with respect to the loading direction in Figure 6b, on the other hand, leads to reduced deformability and brittle fracture behavior since the filament lines detach from each other. A smooth or scaly fracture face is recognizable. Once filament separation begins, it continues along the contact area throughout the specimen, leading to sudden failure.
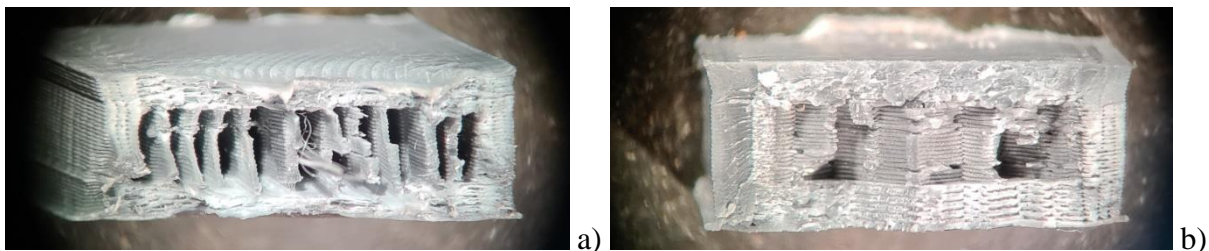
Source: Own work

Fig. 6: *Macro images of the fracture faces of a tensile specimen with a) 40% concentric structure and b) 40% grid structure*

Structures with a high filament content that are loaded in the direction of deposition also achieve higher fracture strain values, e.g. in the case of gyroid and concentric. Triangles, grids and cube subdivision are, on the other hand, structures where the filaments are loaded at an angle of up to 90° to the direction of deposition, resulting in lower fracture strains. The influence of the infill density can be neglected in this respect.

Conclusion

In summary, a linear relationship between the infill density and the Young's modulus as well as the tensile strength can be stated. This applies to all structures under investigation. At the same time, it has been noted that the Young's modulus is influenced by the structures and infill densities and does not represent a pure material parameter.

Furthermore, the applied manufacturing process determines the resulting microstructure, which, in turn, significantly influences the mechanical properties. Different deposition directions of the filament lines during the manufacturing process lead to a dependence of the mechanical properties on the tensile direction to the position of the filament lines. The best results are achieved if the tensile direction is in the direction of deposition since the load-bearing cross-section is at its maximum in this case. When positioned at an angle of up to 90° to the direction of deposition, the load-bearing cross-section is reduced to the connection between the individual filament lines. The fracture strain does not show a significant dependence on the infill density or structure.

Acknowledgements

Literature

[1] ALAFAGHANI, A.; QATTAWI, A.; ALRAWI, B.; GUZMAN, A.: Experimental Optimization of Fused Deposition Modelling Processing Parameters: A Design-for-Manufacturing Approach. *Procedia Manufacturing*. DOI: 10.1016/j.promfg.2017.07.079

[2] LUZANIN, O.; MOVRIN, D.; PLANCAK, M.: Effect of layer thickness, deposition angle, and infill on maximum flexural force in FDM-built specimens. *Journal for Technology of Plasticity*. 2014, Vol. 39, Issue 1, pp. 49–57. ISSN 0354-3870.

[3] ALAFAGHANI, A.; QATTAWI, A.: Investigating the effect of fused deposition modeling processing parameters using Taguchi design of experiment method. *Journal of Manufacturing Processes*. DOI: 10.1016/j.jmapro.2018.09.025

[4] FERNANDEZ-VICENTE, M.; CALLE, W.; FERRANDIZ, S.; CONEJERO, A.: Effect of Infill Parameters on Tensile Mechanical Behavior in Desktop 3D Printing. *3D Printing and Additive Manufacturing*. DOI: 10.1089/3dp.2015.0036

[5] JOHNSON, G. A.; FRENCH, J. J.: Evaluation of Infill Effect on Mechanical Properties of Consumer 3D Printing Materials. *Advances in Technology Innovation*. 2018, Vol. 3, Issue 4, pp. 179–184. ISSN 2415-0436. e-ISSN 2518-2994.

[6] RODRÍGUEZ-PANES, A.; CLAVER, J.; CAMACHO, A. M.: The Influence of Manufacturing Parameters on the Mechanical Behaviour of PLA and ABS Pieces Manufactured by FDM: A Comparative Analysis. *Materials*. DOI: 10.3390/ma11081333

[7]   RISMALIA, M.; HIDAJAT, S. C.; PERMANA, I. G. R.; HADISUJOTO, B.; MUSLIMIN, M.; TRIAWAN, F.: Infill pattern and density effects on the tensile properties of 3D printed PLA material. *Journal of Physics: Conference Series*. DOI: 10.1088/1742-6596/1402/4/044041

[8]   PANDZIC, A.; HODZIC, D.; MILOVANOVIC, A.: Effect of Infill Type and Density on Tensile Properties of PLA Material for FDM Process. In: Katalinic, B. (ed.), *Proceedings of the 30th DAAAM International Symposium on Intelligent Manufacturing and Automation*. DAAAM International, Vienna, Austria, 2019, pp. 0545–0554. ISBN 978-3-902734-22-8. ISSN 1726-9679. DOI: 10.2507/30th.daaam.proceedings.074

[9]   CHACÓN, J. M.; CAMINERO, M. A.; GARCÍA-PLAZA, E.; NÚÑEZ, P. J.: Additive manufacturing of PLA structures using fused deposition modelling: Effect of process parameters on mechanical properties and their optimal selection. *Materials & Design*. DOI: 10.1016/j.matdes.2017.03.065

[10]   SUKINDAR, N. A. B.; ARIFFIN, M. K. A. B. M.; BAHARUDIN, B. T. H. T. B.; JAAFAR, C. N. A. B.; ISMAIL, M. I. S. B.: Analysis on the impact process parameters on tensile strength using 3D printer repetier-host software. *ARPN Journal of Engineering and Applied Sciences*. 2017, Vol. 12, Issue 10, pp. 3341–3346. ISSN 1819-6608.

[11]   KOTLINSKI, J.: Mechanical properties of commercial rapid prototyping materials. *Rapid Prototyping Journal*. DOI: 10.1108/RPJ-06-2012-0052

[12]   LANZOTTI, A.; GRASSO, M.; STAIANO, G.; MARTORELLI, M.: The impact of process parameters on mechanical properties of parts fabricated in PLA with an open-source 3-D printer. *Rapid Prototyping Journal*. DOI: 10.1108/RPJ-09-2014-0135

Dipl.-Ing. Wolfgang Förster; Prof. Dr. Thomas Pucklitzsch; Prof. Dr.-Ing. habil. Daniela Nickel

Vliv různých výplňových struktur na mechanické vlastnosti v přídavné výrobě

Kromě vnějšího pláště nejvíce přispívají k mechanické integritě aditivně vyráběné součásti vnitřní struktury. Za účelem zkoumání vlivu geometricky odlišných vnitřních struktur a hustoty výplně byly na Youngově modulu pružnosti v tahu a deformaci při přetržení připraveny vzorky kyseliny polymléčné (PLA) pomocí modelování fúzního nanášení a testovány při pokojové teplotě. Významný vliv na mechanické vlastnosti měla hustota výplně, výrobní proces a výsledná mikrostruktura. Stručně řečeno, poloha mikrostruktury vzhledem ke směru zatížení byla shledána jako významný faktor vlivu.

Einfluss verschiedener Innenstrukturen auf die mechanischen Eigenschaften in der additiven Fertigung

Neben der äußeren Hülle haben die Innenstrukturen den größten Anteil an der mechanischen Integrität eines additiv gefertigten Bauteils. Um den Einfluss der geometrisch verschiedenen Innenstrukturen und Füllgrade auf Elastizitätsmodul, Zugfestigkeit und Bruchdehnung zu untersuchen, wurden Zugproben aus Polylactid (PLA) mit dem Schmelzschichtverfahren hergestellt und bei Raumtemperatur geprüft. Es konnte ein signifikanter Einfluss des Füllgrades, des Fertigungs-verfahrens und der resultierenden Mikrostruktur auf die mechanischen Eigenschaften beobachtet werden. Zusammenfassend zeigt sich dabei die Lage der Mikrostruktur zur Belastungsrichtung als maßgeblicher Einflussfaktor.

Wpływ różnych struktur wypełniających na mechaniczne właściwości w produkcji addytywnej

Oprócz zewnętrznej obudowy na integralność mechaniczną w największym stopniu wpływają addytywnie wytwarzane elementy struktury wewnętrznej. W celu zbadania wpływu zróżnicowanych geometrycznie struktur wewnętrznych i gęstości wypełnienia na Moduł Younga, określający sprężystość przy rozciąganiu i ściskaniu, były w momencie zerwania metodą modelowania uplastycznionym tworzywem (FDM) przygotowane próbki polikwasu mlekowego (PLA), które badano w temperaturze pokojowej. Znaczący wpływ na właściwości mechaniczne miała gęstość wypełnienia, proces produkcji oraz końcowa mikrostruktura. Podsumowując, wykazano, że położenie mikrostruktury w stosunku do kierunku obciążenia jest ważnym czynnikiem decydującym.

FUNGAL BIODIVERSITY AT THE GRAVEYARD "*GOTTESACKER*" IN HERRNHUT (UPPER LUSATIA, SAXONY)

Alexander Karich[1]; **René Ullrich**[2]; **Martin Hofrichter**[3]
TU Dresden, International Institute Zittau,
Department of Bio- and Environmental Sciences,
Markt 23, 02763 Zittau, Germany
e-mail: [1]alexander.karich@tu-dresden.de; [2]rene.ullrich@tu-dresden.de;
[3]martin.hofrichter@tu-dresden.de

Abstract

The *Gottesacker* ("God's acre") in Herrnhut (Upper Lusatia, Saxony) has been a graveyard for almost 300 years. G. ZSCHIESCHANG has mapped its fungal community since the 1960ies. Combining these findings and those of other mycologists, mycological data that cover about 55 years are reported here. In this context, we discuss the fungal biodiversity with special emphasis on CHEGD species (***Clavariaceae-Hygrocybe-Entoloma-Geoglossaceae-Dermoloma***). These species are used to classify and assess the conservation value of grasslands by monitoring their fungal communities. According to the determined CHEGD profile, the *Gottesacker* graveyard is ranked as a grassland of international importance. In addition, we present macroscopic and microscopic characteristics of two rare CHEGD species: *Entoloma brunneosericeum* and *Clavaria messapica*. These are the first records of both species for Germany and Saxony, respectively.

Keywords

CHEGD; *Clavaria messapica*; *Entoloma brunneosericeum*; *Hygrocybe*; Biodiversity; Fungi.

Introduction

During the last decades, a serious loss of biodiversity has been recorded worldwide [1]. The human-driven loss of biological diversity has numerous causes, for example, pollution due to fossil fuels and crude oil-based chemicals and changes in land use including overgrazing, deforestation, urbanization and the cultivation of monocultures. Especially the latter is associated with the usage of biocides including fungicides as well as chemical fertilizers causing eutrophication. Grassland fungi are particularly affected by fertilization – not only through the direct application of fertilizers – but also via passive input through rain, surface water and wind. The so-called CHEGD species represent fungi that are highly sensitive to such inputs and are hence appropriate for biomonitoring purposes; the acronym stands for ***Clavariaceae-Hygrocybe-Entoloma-Geoglossaceae-Dermoloma*** [2]. It is thought that these praticolous fungal genera are well adapted to nutrient-poor environments because of their biotrophic [3, 4, 5] and/or endophytic (in higher plants) lifestyles [6]. Not least, this may explain why CHEGD fungi respond highly sensitive to external nutrient impact, which makes them suitable bioindicators for unimproved "natural" grasslands.

Because of intensive farming (industrial agriculture) in the German part of the Euroregion "Neisse-Nisa-Nysa" during the last decades, only few locations of unimproved grasslands have remained, e.g. in the Zittau Mountains (*Zittauer Gebirge*) and the Upper Lusatian Heath and Pond Landscape (*Niederlausitzer Heide- und Teichlandschaft*). On the other hand, artificial man-made locations and landscapes, such as meadows in parks and cemeteries, can

be low in nutrients as well, depending on horticulture management, and have an astonishing number of rare fungal grassland species [7]. Such an interesting locality is the graveyard *Gottesacker* ("God's acre") that has been situated on the Hutberg in Herrnhut[1] (Saxony) since 1730. Remarkably, Herrnhut is renowned for three important mycologists. LUDWIG LEWIS DAVID VON SCHWEINITZ and JOHANN BAPTISTA VON ALBERTINI wrote the treatise *"Conspectus fungorum in Lusatiae Superioris agro Niskiensi crescentium, e methodo Persooniana"* in 1805 [8], describing 127 new fungal species. Further, in the early 1960s, the mycologist GERHARD ZSCHIESCHANG[2] began an inventory of the funga of Saxony with a focus on East Saxony (Upper Lusatia), part of the Euroregion "Neisse-Nisa-Nysa", which included the *Gottesacker* graveyard in Herrnhut.

1   Research Subject

Since 2016, the authors of this article have been regularly surveying the *Gottesacker* area to record the funga, with a special focus on CHEGD species. Our results and findings are presented in tabular form and discussed in terms of the available data. Remarkable fungal species are described in detail, including their macroscopic and microscopic characteristics.

2   Material and Methods

2.1   Locality

The graveyard *Gottesacker* (14° 44' 54,9" E; 51° 1' 13,68" N) is about 40,000 m² in size and located in the eastern part of Herrnhut, a town in the Upper Lusatia region 25 km southwest of Görlitz and part of the "Lusatian Highlands" (German *Lausitzer Bergland*, Upper Sorbian *Łužiske hory*) at an altitude of about 350 m. The geology of the region around Herrnhut includes granite in deeper layers and surface clay at the top, but the latter have been strongly influenced by human activities and cannot be ascribed in detail for the graveyard; thus, lime-rich and sandy sections cannot be excluded. The local climate ranges between oceanic and humid continental climate. Respective meteorological data recorded between 1961 and 1990 (station Herrnhut) were as follow: 688 mm average rainfall with maxima in August (75 mm) and average temperature 7.7 °C (- 2.1 °C January to 16.6 °C July). Unfortunately, for the last three decades, no climate data are available for Herrnhut. Ostritz, about 13 km east of Herrnhut, had an average rainfall of 636 mm (1991-2020) with its maximum in July (86 mm). In addition, with regard to temperature, we refer to data from Görlitz (1991-2020) with an average of 9.3 °C (- 0.2 °C January to 18.9 °C July).

2.2   Morphological Studies

Fresh specimen were studied with a light microscope (Zeiss Axio scope). Hand cut thin sections were examined microscopically by squash mounts. Fresh material was inspected in water. Dried material was re-examined in 5% KOH. Measurements of spores were taken from a spore print on stems of dried material (except for *Clavariaceae*). All other features where measured on re-hydrated material in 5% KOH. Measurements were conducted manually. Microscopic drawings are re-drawn in CorelDraw Graphics Suite from pictures taken with a Canon EOS 60D.

---

[1] The town Herrnhut was founded by Protestant religious refugees from Moravia ('Unity of the Brethren') under the patronage of NIKOLAUS LUDWIG GRAF VON ZINZENDORF in 1722.

[2] * 8. March 1931 in Bernsdorf; † 7. November 2012 in Herrnhut

2.3 DNA Extraction, Amplification and Sequencing

DNA extraction was performed according to standard methods with the Plant DNA Mini Kit (VWR, peqlab). The ITS region (ITS1, 5.8S rRNA gene, ITS2) as well as parts of the 28S rRNA gene region were amplified by PCR using the standard primer pairs ITS4/5 and LR0/6 (White et al. [38]). PCR products were SANGER sequenced by LGC Genomics (Berlin, Germany). For comparison, sequences from the databases GenBank [9] and UNITE [10] were used.

3 Results

3.1 List of Documented Species

All recorded CHEGD taxa (including varieties and formae) are listed in Table 1 (based on the DgfM database [11] and own findings). The list includes all records made by ZSCHIESCHANG (his last entry, *Entoloma chlybaeum* var. *lazulinum*, dated 20 July 2008) and records made by other mycologists after his death, beginning with *Cuphophyllus berkeleyi* recorded by HARDKTE in 2015. The list of CHEGD taxa solely collected by ZSCHIESCHANG contains 38 and the overall list 50 species (compare Table 2). The species determination was done using morphological characters, unless otherwise specified in the article.

Tab. 1: *List of CHEGD taxa (including subspecies and all recorded species of the genus Entoloma) reported for the "Gottesacker" graveyard in Herrnhut;* records from 1964 until 2008 *(Zschieschang) / records reported* after 2008 until 2020*, paragraph "§" marks dubious records, asterisk "*" marks species regarded as grassland Entoloma* spp.

Taxon	Rec.	Taxon	Rec.
Clavariaceae		*Entoloma* Fr. ex P. Kumm.	
		*E. anatinum (Lasch: Fr.) Donk	0/1
Clavaria L.		**E. asprellum* (Fr.) Fayod	0/1
C. fragilis Holmsk.: Fr.	2/0	**E. brunneosericeum* Noordel., Vila, F. Caball. & E. Suárez	0/1
C. messapica Agnello, Kautman. & M. Carbone	0/1	**E. chalybaeum* (Fr.) Noordel.	3/2
		*E. chalybaeum var. *lazulinum* (Fr.) Noordel.	2/0
Clavulinopsis Overeem		*E. clypeatum* (L.) P. Kumm.	1/0
C. corniculata (Schaeff.: Fr.) Corner	4/1	**E. conferendum* (Britzelm.) Noordel	8/1
C. helvola (Pers.: Fr.) Corner	1/3	**E. dysthaloides* Noordel.	1/0
C. laeticolor (Berk. & M.A. Curtis) R.H. Petersen	1/1	**E. favrei* Noordel.	1/1§
C. luteoalba (Rea) Corner	1/1	**E. infula* (Fr.) Noordel.	1/1
C. umbrinella (Sacc.) Corner	0/1	*E. juncinum* (Kühner & Romagn.) Noordel.	1/0
		*E. jubatum (Fr.) P. Karst.	0/1
Ramariopsis (Donk) Corner		**E. sarcitulum* (Orton) Noordel.	0/1
R. kunzei (Fr.) Corner	1/1	**E. lepidissimum* (Svrček) Noordel.	0/1
		E. lividoalbum (Kühner & Romagn.) Kubička	12/1
Hygrocybaceae		**E. lucidum* (P.D. Orton) M.M. Moser	1/0
		*E. neglectum (Lasch: Fr.) M.M. Moser	2/0
Cuphophyllus (Donk) Bon		**E. nitens* (Velen.) Noordel.	6/0
C. angustifolius (Murrill) Bon	1/0	**E. papillatum* (Bres.) Dennis	13/2
C. berkeleyi (P.D. Orton & Watling) Bon	0/2	**E. pleopodium* (Bull.) Noordel.	1/0
C. borealis (Peck) Bon	1/0§	**E. porphyrophaeum* (Fr.) P. Karst.	7/0
C. cereopallidus (Clémençon) Bon	1/0	**E. pseudoturci* Noordel.	0/1§
C. lacmus (Schumach.) Bon	2/0	*E. rhodopolium* (Fr.) P. Kumm.	2/0
C. pratensis (Pers.: Fr.) Bon	16/5	**E. sericellum* (Fr.) P. Kumm.	2/1
C. virgineus (Wulfen) Kovalenko	14/4	**E. sericeum* (Bull. ex Mérat) Quél.	12/4
		E. sordidulum (Kühner & Romagn.) M.M. Moser	2/0
Gliophorus Herink		*E. tenellum* (J. Favre) Noordel.	
G. irrigatus (Pers.) A.M. Ainsw. & P.M. Kirk	12/1	**E. undatum* (Gillet) M.M. Moser	1/0
G. psittacinus (Schaeff.: Fr.) Herink	9/3	**E. velenovskyi* Noordel.	1/1
		E. vernum S. Lundell	0/1
Hygrocybe (Fr.) P. Kumm.		**E.* spec. undescribed species subg. *Nolanea*	6/0
H. ceracea (Wulfen: Fr.) P. Kumm.	8/2		0/1
H. coccinea (Schaeff.: Fr.) P. Kumm.	16/2		
H. conica (Schaeff.) P. Kumm.	6/5	***Geoglossaceae***	
H. conica f. *pseudoconica* (J.E. Lange) Arnolds	0/1		
H. glutinipes (J.E. Lange) R. Haller Aar.	2/0	*Glutinoglossum* Hustad, A.N. Mill., Dentinger &	
H. insipida (J.E. Lange) M.M. Moser	1/0	P.F. Cannon	

H. persistens (Britzelm.) Singer	4/0	*G. glutinosum* (Pers.) Hustad, A.N. Mill., Dentinger & P.F. Cannon	0/1
H. quieta (Kühner) Singer	2/0		
H. vitellina (Fr.) P. Karst.	3/1		
		Dermoloma s.l.	
Neohygrocybe Herink			
N. nitrata (Pers.) Kovalenko	3/0	*Dermoloma* J.E. Lange ex Herink	
		D. cuneifolium (Fr.) P. D. Orton	5/3
Entoloma s.l.			
Entocybe T.J. Baroni, V. Hofstetter & Largent			
E. turbida (Fr.) T.J. Baroni, V. Hofst. & Largent	3/0		
*E. vinacea (Scop.) T.J. Baroni, V. Hofst. & Largent	1/0		

Source: Own and [11]

Source: All photographs taken from locality by A. Karich.

Fig. 1: *Clavulinopsis luteoalba* (A), *Clavulinopsis corniculata* (B), *Clavulinopsis umbrinella* (C), *Hygrocybe ceracea* (D), *Entoloma pseudoturci* (E), *Entoloma sarcitulum* (F), *Entoloma chalybaeum* (G), *Entoloma asprellum* (H), *Hygrocybe coccinea* (I), *Gliophorus psittacinus* (J), *Entoloma sericellum* (K), *Entoloma infula* (L), *Entoloma papillatum* (M), *Entoloma favrei* (N), *Dermoloma cuneifolium* (O) and *Glutinoglossum glutinosum* (P).

3.2 Description of Selected Species

Two lately erected species were selected to be described in detail. These are to our knowledge the only descriptions next to their original diagnosis.

3.2.1 *Entoloma brunneosericeum* Noordel., Vila, F. Caball. & E. Suárez, Fungi non Delineati 66: 31 (2013)

Pileus 9-27 mm in diameter, convex to applanate with a broad umbo, not to hardly striate at margin only, appearing waxy, not hygrophanous, almost uniformly dark brown (R: 70, G: 65, B: 45), margin slightly involute and sometimes with fine greyish-white fibrils.

Lamellae 22-30 with 1-5 lamellulae, crowded, emarginated to almost free, slightly ventricose, sordid greyish, lamellar edge concolorous. Smell inconspicuously farinaceous.

Stem 40-90 x 2-5 mm, overall densely silvery striate, hollow.

Spores (7-)8-$\underline{8.4}$-9(-9.5) x (6.5-)7-$\underline{7.65}$-8 µm, Q = 1.0-$\underline{1.09}$-1.19, mostly isodiametrical, only some slightly subisodiametrical, with 6 (7) rounded angles. Basidia 4-spored, 35-50 x 10-12 µm.

Lamellar trama composed of long elements. Pileipellis, a cutis made of 5-10 µm wide hyphae, in subpellis up to 30 µm wide, pigment abundant coarsely incrusted, brown, also infrequently intracellular (possibly vacuolar) brown, incrusted hyphae reaching into pileitrama. Hyphae in stipitipellis coarsely incrusted. Clamps restricted to hymenium only.

Studied material:

15.09.2017, Germany, Herrnhut, graveyard, in the meadow, MTB 4954.43, leg et. det. A. KARICH and R. ULLRICH, voucher No. IHI-17Ent01, ITS MW786739.

Comments: According to its original description, *E. brunneosericeum* is restricted to montane to subalpine *Pinus* forests [12]. Besides ours, another collection from an alpine pasture in Protomagno (Italy) [13], has already given indication for its preference of unimproved grasslands. However, the collection illustrated herein is the first one from a colline area and the first record of this species in Germany. The respective ITS sequence was found to be identical to the sequence of the holotype (JX454894).

Source: Photographs and drawings by A. Karich.

Fig. 2: *Entoloma brunneosericeum* – macroscopic characters *in situ* (left, bar = 1cm) – basidia (A) and spores (B), bars 10 µm.

### 3.2.2 *Clavaria messapica* Agnello, Kautman. & M. Carbone, Rivista di Micologia 57 (3): 197 (2015)

Basidiocarps clavate to cylindric-fusoid, slightly curved or twisted, tapering towards base, 40-70 mm x 2.5-5 mm, occasionally single branched, apex rounded, light rose colored, freeze-dried material white-rose, surface rugulose; sterile stem part slightly darker and only hardly distinguishable from fertile club, glabrous to finely pubescent. Flesh a little darker than surface and a bit crumbling. No significant smell or taste observed on fresh specimen, odor of dried material somewhat reminiscent of cocoa.

Spores (6-)6.5-7.0-7.5(-8) x 4-4.3-5 μm, Q = 1.5-1.63-1.8, heteromorphic cylindric, ellipsoid, ovoid, sometimes slightly phaseoliform or constricted, with an evident apiculus, not ornamented. Basidia 2- and 4-spored, 55-75(-80) x 6-9 μm, long, slenderly clavate, often guttulate, at the base frequently with loop like clamp connections. Sterile, thin-walled cystidioid elements present in hymenium, 30 – 70 x 2.5-6 μm, cylindrical, curved, flexuously-twisted to clavate, with rounded apex, with loop-like clamps. Trama consisting of cylindrical, 5-16 μm wide, clampless, thin-walled and rarely branched hyphae.

Studied material:

01.11.2020, Germany, Herrnhut, graveyard in the meadow, MTB 4954.43, leg et. det. A. KARICH and R. ULLRICH, voucher No. IHI-20Cla01, ITS MW786738, LSU MW786737.

Remarks: In the original description of *C. messapica,* AGNELLO ET AL. reported leptocystida to be present in the hymenium [14]. The authors here compared them with the fairly large cystidia of *Alloclavaria purpurea* (O.F. Müll.: Fr.) B. Dentinger & D.J. McLaughlin, but on the other hand, they were mentioned to be much smaller than the basidia (30-55 x 3-5.5[-6] μm) and did not exceed the hymenium. In contrast, the photographs of micro characters in AGNELLO et al. [14] depict hyphae named cystidia that seem to be as long as the basidia. We observed many sterile cystidioid elements that could represent thin leptocystidia in the hymenium. However, these elements could be just as well transition states of young basidia (often referred to as basidioles, compare the discussion on *Lamelloclavaria petersenii* ADAMčíK & BIRKEBAK in KARICH & ULLRICH [15]). It should be noted that we did not observe any cystidioid element without loop-like clamps at the base. Of course, this raises the question of how the macroscopically similar *C. incarnata* and *C. messapica* can be distinguished morphologically, if the characteristic hymenialcystidia will not be present (or even if they are hardly to differentiate as such). As already mentioned by AGNELLO et al. [14], the spore size can be a good feature to discriminate between *C. incarnata* and *C. messapica*. The spores of the latter are never longer than 8 μm, while spores of *C. incarnata* may reach 10 μm in length. Unfortunately, the variation of spore length of *C. incarnata* seems to include the spore size of *C. messapica*. This becomes clear when the spore measurements of *C. incarnata* in JÜLICH [16], KNUDSEN et al. [17] and CORNER [18] are taken into account. Thus, it can be assumed that specimen of *C. messapica* were misinterpreted in the past. Yet, AGNELLO et al. [14] mentioned that specimen of *C. incarnata* had turned yellowish when dried whereas those of *C. messapica* stayed rose without any shade of yellow. The basidiocarps of our (freeze-dried) collection faded a little to white-rose, not becoming yellowish. Another feature that is worth mentioning was the cocoa-like smell of dried specimen from Herrnhut, an odor that was not reported for *C. incarnata* so far. Nevertheless, the LSU sequence of the Herrnhut specimen is 99.52% identical to that of the type specimen of *C. messapica* (NG_068754).
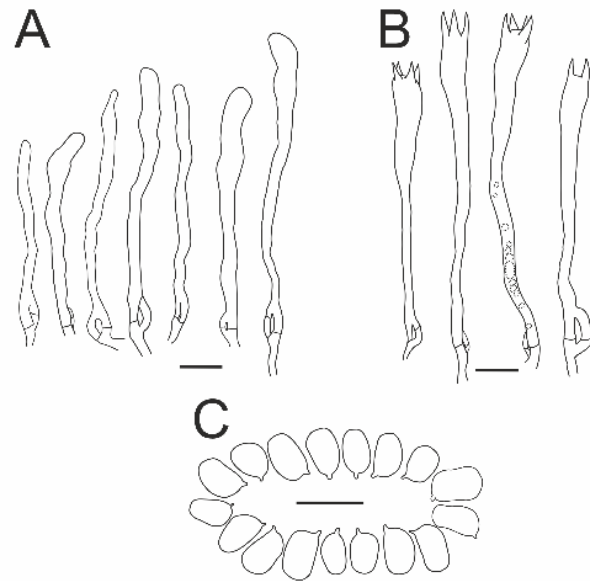
Source: Photograph and drawings by A. Karich.

Fig. 3: *Clavaria messapica* – macroscopic characters *in situ* (left) – basidioles (A), basidia (B) and spores (C), bars 10 μm.

4 Discussion

In addition to botanical (herbal) inventories, fungi surveys should be considered when determining whether grasslands are in need of protection. The relevance of CHEGD species for monitoring the conservation value of grasslands is indisputable [19-22]. The former concept of CHEG species of NITARE [20] and ROTHEROE [22] was extended by representatives of the genera *Dermoloma* and *Camarophyllus* as well by the single species *Porpoloma metapodium* (CHEGD) in GRIFFITH et al. [2]. With regard to species of the genus *Entoloma*, GRIFFITH et al. [2] excluded those that are listed as woodland dwellers according to LEGON & HENRICI [23], and ROTHEROE [22] included "grassland species of the family *Entolomataceae*" in his survey without further specifying the term. While it is reasonable to exclude species that certainly form ectomycorrhiza with *Rosaceae*, e.g. *E. clypeatum*, *E. aprile* and *E. saepium* [24, 25], the boundary between forest and grassland species is rather blurred. Some species that appear in GRIFFITH'S CHEGD checklist have been reported for both habitats, e.g. *E. conferendum* and *E. undatum* or are – according to NOORDELOOS [25] – even linked to woodlands, e.g. *E. lampropus*. Even NITARE [20] listed *E. juncinum*, a species that surely has rather low requirements on its habitat; it grows "frequently under *Urtica* in nitrogen-rich habitats" [25: p. 246]. This bivalence with regard to the habitat (woodland vs. grassland) has been observed for other members of the CHEGD taxa as well, e.g. for species of the *Clavariaceae* [26, 27] *Hygrocybe* s.l. [3, 28] and *Microglossum* spp. belonging to *Geoglossaceae* [29, 30]. In the genus *Entoloma*, all species from the subgenera *Leptonia* and *Trichopilus* as well as some from the subgenus *Nolanea* are regarded as grassland dwellers [25, 31]. In the future, however, a comprehensive list of grassland species will be needed to ensure the correct interpretation of CHEGD lists.

A total of 33 *Entoloma* species have been recorded in the *Gottesacker* graveyard in recent decades, but only 23 can be considered praticolous and of these, again, two recorded taxa should be labeled "dubious", namely *E. favrei* and *E. pseudoturci*. The first taxon will probably have to be included into *E. clandestinum* s.s. Already LUDWIG [32] reclassified *E. papillatum* under *E. clandestinum.* This was later approved by molecular studies by

KOKKONEN [33], who included *E. kerocarpus*, as well. We collected some specimens that were determined to be *E. favrei* (mainly because of the capitate caulocystidia) but were found to belong to *E. clandestinum* based on the ITS sequence (data not published; compare figures 1 M and N). The second doubtful species, *E. pseudoturci*, was determined on the basis of morphological characters (compare figures 1 E and F), but its partial ITS-Sequence (approx. 150 bp length – data not shown) was close to that published by KOKKONEN [33] for *E.* aff. *sarcitulum*, a species that forms a complex with *E. longistriatum* and *E. sarcitulum* and requires further investigation.

Noteworthy is the appearance of five whitish to cream-colored species of the genus *Cuphophyllus* (formerly *Hygrocybe*), *i.e.* *C. angustifolius*, *C. berkeleyi*, *C. borealis*, *C. cereopallidus*, *C. virgineus*. While BOERTMANN [28] recognizes only the latter at the species level, other authors consider all five to be separate species [34-37]. *C. borealis*, however, seems to represent a dry form of *C. virgineus,* as already pointed out by HARDTKE [36] and BOERTMANN [28] and was thus marked as "dubious species" on the list.

For the time being, we include all these doubtful records in our CHEGD list, but being aware of possible taxonomic changes in the near future.

Tab. 2: *Evaluation scheme for CHEGD species modified according to GRIFFITH et al. [2] and LÜDERITZ [27] with regard to records at the "Gottesacker" solely made by ZSCHIESCHANG and total records in brackets (Z./total)*

Value ranking	*Clavaria-ceae*	*Hygro-cybe* **s.l.**	*Entoloma* **s.l.**	*Geoglossa-ceae*	*Dermo-loma*	**Sum**
1. International	**8**+ (6/8)	**15**+ (17/18)	**15**+ (15/23)	**4**+	**4**+	**46**+ (38/51)
2. National	**5**+	**10**+	**10**+	**3**+	**3**+	**31**+
3. Regional	**3**+	**7**+	**6**+	**2**	**2**	**20**+
4. Local	**2**	**4**+	**3**+	**1**	**1**	**11**+
5. Municipal	**1**	**2**+	**2**+	**1**(0/1)	**1**(1/1)	**7**+
6. Not deserving protection	**0**	**0-1**	**0-1**	**0**	**0**	**0-2**

Source: Own

The CHEGD profile of the *Gottesacker* solely based on ZSCHIESCHANG'S records can be described as: C6 H17 E15 G0 D1 (in total 38 species). Updated with records post ZSCHIESCHANG, the profile is: C8 H18 E23 G1 D1 (in total 51 species). Following the evaluation-scheme of GRIFFITH et al. [2] and its modification according to LÜDERITZ [27], the *Gottesacker* is to be classified a grassland of international value (Table 2). In addition to the outstanding CHEGD profile, we want to point out the noteworthy records of two species, of which one, *E. brunneosericeum*, is new to Germany and represents – to our knowledge – the first record north of the Alps. The other remarkable species, *C. messapica*, is new to Saxony and represents the second record for Germany. There is another currently undescribed *Entoloma* sp. from the *Gottesacker* graveyard, which we have also found at another high-value grassland (in the Zittau Mountains [38]), but its description is still pending.

Eventually, we would like to emphasize that the three most valuable grasslands (in terms of fungal diversity) in Upper Lusatia are "meadows" in parks, *i.e.* the herein described *Gottesacker* in Herrnhut, then a recently reported park lawn in Lückendorf [7, 15] and the "Azalea and Rhododendron Park Kromlau" with outstanding records of *Clavria zollingeri* and *Hygrocybe punicea* [11].

Conclusion

The CHEGD profile of the *Gottesacker* graveyard, which is based on survey-data of over 50 years, is in fact an outstanding refuge for rare fungal species and can be ranked as habitat of international importance. The two noteworthy records of *E. brunneosericeum* and *C. messapica* underline the uniqueness of this highly valuable, unimproved grassland.

Acknowledgements

Literature

[1] CARDINALE, B. J.; DUFFY, J. E.; GONZALEZ, A.; HOOPER, D. U.; PERRINGS, Ch.; VENAIL, P.; NARWANI, A.; MACE, G. M.; TILMAN, D.; WARDLE, D. A.; KINZIG, A. P.; DAILY, G. C.; LOREAU, M.; GRACE, J. B.; LARIGAUDERIE, A.; SRIVASTAVA, D. S.; NAEEM, S.: Biodiversity loss and its impact on humanity. *Nature*. DOI: 10.1038/nature11148

[2] GRIFFITH, G. W.; GAMARRA, J. G. P.; HOLDEN, E. M.; MITCHEL, D.; GRAHAM, A.; EVANS, D. A.; EVANS, S. E.; ARON, C.; NOORDELOOS, M. E.; KIRK, P. M.; SMITH, S. L. N.; WOODS, R. G.; HALE, A. D.; EASTON, G. L.; RATKOWSKY, D. A.; STEVENS, D. P.; HALBWACHS, H.: The international conservation importance of Welsh 'waxcap' grasslands. *Mycosphere*. DOI: 10.5943/mycosphere/4/5/10

[3] HALBWACHS, H.; KARASCH, P.; GRIFFITH, G. W.: The diverse habitats of Hygrocybe – peeking into an enigmatic lifestyle. *Mycosphere*. DOI: 10.5943/mycosphere/4/4/14

[4] HALBWACHS, H.; EASTON, G. L.; BOL, R.; HOBBIE, E. A.; GARNETT, M. H.; PERŠOH, D.; DIXON, L.; OSTLE, N.; KARASCH, P.; GRIFFITH, G.W.: Isotopic evidence of biotrophy and unusual nitrogen nutrition in soil-dwelling Hygrophoraceae. *Environmental Microbiology*. DOI: 10.1111/1462-2920.14327

[5] RUTHSATZ, B.: Was haben Pilze wie die Saftlinge (Gattung Hygrocybe s. l.) auf magerem Grünland zu suchen? *Tuexenia*. DOI: 10.14471/2018.38.007

[6] TELLO, S. A.; SILVA-FLORES, P.; AGERER, R.; HALBWACHS, H.; BECK, A.; PERŠOH, D.: Hygrocybe virginea is a systemic endophyte of Plantago lanceolata. *Mycological Progress*. DOI: 10.1007/s11557-013-0928-0

[7] KARICH, A.; KELLNER, H.; SCHMIDT, M.; ULLRICH, R.: Ein bemerkenswertes Mykotop im Zittauer Gebirge mit Microglossum rufescens als Erstnachweis für Deutschland. *Boletus*. 2015, Vol. 36, Issue 2, pp. 151–163.

[8] DÖRFELT, H.; HEKLAU, H.: *Die Geschichte der Mykologie*. Einhorn-Verlag Dietenberger, Schwäbisch Gmünd, 1998. ISBN 3927654442.

[9] NCBI: *GenBank*. [online]. 2021. [accessed 2021-03-09]. Available from WWW: https://www.ncbi.nlm.nih.gov/

[10] NILSSON, R. H.; LARSSON, K.-H.; TAYLOR, A. F. S.; BENGTSSON-PALME, J.; JEPPESEN, T. S.; SCHIGEL, D.; KENNEDY, P.; PICARD, K.; GLÖCKNER, F. O.; TEDERSOO, L.; SAAR, I.; KÕLJALG, U.; ABARENKOV, K.: The UNITE database for molecular identification of fungi: handling dark taxa and parallel taxonomic classifications. *Nucleic Acids Research*. DOI: 10.1093/nar/gky1022

[11] DGfM: *Pilze Deutschlands*. [online]. 2021. [accessed 2021-03-09]. Available from WWW: http://www.pilze-deutschland.de/

[12] VILA, J.; CARBÓ, J.; CABALLERO, F.; CATALÀ, S.; LLIMONA, X.; NOORDELOOS, M. E.: A first approach to the study of the genus Entoloma subgenus Nolanea s.l. using molecular and morphological data. *Fungi non Delineati*. 2013, Vol. 66 (Studies on Entoloma): Edizioni Candusso, Alassio. ISSN 1128-6008.

[13] DONDL, M.: *Hias' Schwammerlseiten*: Entoloma: Nr. 13: Entoloma brunneosericeum Noordel., Vila, F. Caball. & E. Suárez. [online]. 2021. [accessed 2021-03-09]. Available from WWW: http://www.interhias.de/schwammerlseiten/bestimmungen/2014/entoloma/entoloma.html#ank13

[14] AGNELLO, C.; KAUTMANOVÁ, I.; CARBONE, M.: Clavaria messapica, una nuova specie del sud della Puglia. *Rivista di Micologia*. 2014, Vol. 3, pp. 195–210.

[15] KARICH, A.; ULLRICH, R.: Lamelloclavaria petersenii, a Clavariaceae with agaric hymenophor-First German record. *Boletus*. 2019, Vol. 40, Issue 1, pp. 17–23.

[16] JÜLICH, W.: *Die Nichtblätterpilze, Gallertpilze und Bauchpilze*. VEB Gustav Fischer Verlag, Jena, 1984. ISBN 3437202820.

[17] KNUDSEN, H.; SHIRYAEV, A. G.; KAUTMANOVÁ I.: Clavaria L.: Fr. In: Knudsen H.; Vesterholt J. (eds), *Funga Nordica*, 2nd edition. 2018. ISBN 9788798396130.

[18] CORNER, E. J. H.: *A Monograph of Clavaria and Allied Genera*. Oxford University Press, London, 1950. ISBN 8121104602.

[19] ARNOLDS, E. J. M.: *Ecology and coenology of macrofungi in grasslands and moist heathlands in Drenthe, the Netherlands*. J. Cramer im AR Grantner Verlag Vaduz, 1981. ISBN 9783768213141.

[20] NITARE, J.: Jordtungor, en svampgrupp pa tillbakagang i naturligafodermarker. *Svensk Botanisk Tidskrift*. 1988, Vol. 82, pp. 341–368.

[21] RALD, E.: Vokshatte som indikatorarter for mykologisk vaerdifulde overdrevslokaliteter. *Svampe*. 1985, Vol. 11, pp. 1–9.

[22] ROTHEROE, M.: *Mycological survey of selected semi-natural grasslands in Carmarthenshire*. Contract Science Report No. 340. Countryside Council for Wales, Bangor, 1999.

[23] LEGON, N. W.; HENRICI, A.: *Checklist of the British & Irish Basidiomycota*. Royal Botanic Gardens, Kew, 2005. ISBN 1842461214.

[24] KOBAYASHI, H.; HATANO, K.: A morphological study of the mycorrhiza of Entoloma clypeatum f. hybridum on Rosa multiflora. *Mycoscience*. DOI: 10.1007/BF02463979

[25] NOORDELOOS, M. E.: *Entoloma, s.l. (Fungi Europaei 5)*. Libreria editrice Giovanna Biella, Saronno, 1992.

[26] CORNER, E. J. H.: *Supplement to "A Monograph of Clavaria and allied Genera"*. Nova Hedwigia, Beihefte, Vol. 33, 1970. ISBN 978-3-768-25433-5.

[27] LÜDERITZ, M.: Kooperation im mykologischen Artenschutz – Hotspot auf Fehmarn entdeckt. In: *Jahresbericht 2016 zur biologischen Vielfalt – Jagd- und Artenschutz*. Ministerium für Energiewende, Landwirtschaft, Umwelt und ländliche Räume des Landes Schleswig Holstein, Kiel, Germany, 2016.

[28] BOERTMANN, D.: *The genus Hygrocybe. 2nd revised edition (Fungi of nordern Europe Vol. 1)*. Narayana Press, Roskilde, 2010. ISBN 9788798358176.

[29] KUČERA, V.; LIZOŇ, P.; TOMŠOVSKÝ, M.; KUČERA, J.; GAISLER, J.: Re-evaluation of the morphological variability of Microglossum viride and M. griseoviride sp. nov. *Mycologia*. DOI: 10.3852/106.2.282

[30] KUČERA, V.; LIZOŇ, P.; TOMŠOVSKÝ, M.: Taxonomic divergence of the green naked-stipe members of the genus Microglossum (Helotiales). *Mycologia*, DOI: 10.1080/00275514.2016.1274620

[31] NOORDELOOS, M. E.: *Entoloma s.l. Supplemento*. Massimo Candusso, Alassio, 2004. ISBN 9788890105746.

[32] LUDWIG, E.: *Pilzkompendium, Bd. 2: Beschreibungen. Die größeren Gattungen der Agaricales mit farbigem Sporenpulver (ausgenommen Cortinariaceae)*. Fungicon Verlag. Berlin, 2007. ISBN 9783940316011.

[33] KOKKONEN, K.: A survey of boreal Entoloma with emphasis on the subgenus Rhodopolia. *Mycological Progress*. DOI: 10.1007/s11557-015-1135-y

[34] CLÉMENÇON, H.: Taxonomische und nomenklatorische Notizen zur Gattung Camarophyllus. *Schweizer Zeitschrift für Pilzkunde*. 1979, Vol. 57, Issue 8, pp. 113–118.

[35] CLÉMENÇON, H.: Kompendium der Blätterpilze: Camarophyllus. *Beihefte zur Zeitschrift für Mykologie*. 1982, Vol. 4, pp. 39–56.

[36] HARDTKE, H. J.: Interessante weissliche Camarophyllus-Arten. *Mykologisches Mitteilungsblatt*. 1985, Vol. 28, pp. 43–46.

[37] CANDUSSO, M.: *Hygrophorus s.l. (Fungi Europaei 6)*. Candusso Edizioni, Alassio, 1997.

[38] WHITE, T. J.; BRUNS, T.; LEE, S.; TAYLOR, J.: Amplification and direct sequencing of fungal ribosomal RNA genes for phylogenetics. In: Innis, M. A.; Gelfand, D. H.; Sninsky, J. J.; White, T. J. (eds.), *PCR Protocols: A Guide to Methods and Applications*. Academic Press, San Diego, 1990. pp. 315–322. DOI: 10.1016/B978-0-12-372180-8.50042-1

Dr. rer. nat. Alexander Karich; Dr. rer. nat. René Ullrich; Prof. Dr. rer. nat. habil. Martin Hofrichter

HOUBOVÉ SPOLEČENSTVÍ NA HŘBITOVĚ „GOTTESACKER" V HERRNHUTU (HORNÍ LUŽICE, SASKO)

„Gottesacker" v Herrnhutu (Horní Lužice, Sasko) je hřbitovem téměř 300 let. G. Zschieschang intenzivně mapoval své houbové společenství od 60. let 20. století. Spojením jeho nálezů a nálezů jiných mykologů zde můžeme analyzovat mykologická data, která zachycují asi 55 let. Biologickou rozmanitost hub posuzujeme se zvláštním důrazem na druhy CHEGD (*Clavariaceae-Hygrocybe-Entoloma-Geoglossaceae-Dermoloma*). Tyto druhy se používají v soupisech ke klasifikaci a k posouzení toho, zda si travnaté porosty zachovávají svou hodnotu. Podle námi určeného profilu CHEGD lze „Gottesacker" zařadit k travním porostům mezinárodního významu. Dále uvádíme makroskopické a mikroskopické charakteristiky dvou vzácných druhů CHEGD: *Entoloma brunneosericeum* a *Clavaria messapica*. Jedná se o první nálezy obou druhů v Sasku (prvního jmenovaného dokonce v celém Německu).

PILZLICHE BIODIVERSITÄT AUF DEM FRIEDHOF "GOTTESACKER" IN HERRNHUT (OBERLAUSITZ, SACHSEN)

Der „Gottesacker" in Herrnhut (Oberlausitz, Sachsen) ist seit fast 300 Jahren ein Friedhof. G. Zschieschang hatte seine Pilzgemeinschaft seit den 1960er Jahren intensiv kartiert. Indem wir seine Erkenntnisse und die anderer Mykologen zusammenführen, können wir hier mykologische Daten analysieren, die etwa 55 Jahre umfassen. Dabei behandeln wir die pilzliche Biodiversität mit besonderem Augenmerk auf den CHEGD-Arten (*Clavariaceae-Hygrocybe-Entoloma-Geoglossaceae-Dermoloma*). Diese Arten werden im Zuge von Inventarisierungen herangezogen, um den Erhaltungswert von Grünland zu klassifizieren und zu bewerten. Entsprechend dem von uns ermittelten CHEGD-Profil ist der "Gottesacker" als Grünland von internationaler Bedeutung einzustufen. Darüber hinaus präsentieren wir makroskopische und mikroskopische Charakteristika von zwei seltenen CHEGD-Arten: *Entoloma brunneosericeum* und *Clavaria messapica*. Dies sind die Erstnachweise beider Arten für Deutschland bzw. Sachsen.

ZBIOROWISKO GRZYBÓW NA CMENTARZU „GOTTESACKER" W HERRNHUT (GÓRNE ŁUŻYCE, SAKSONIA)

„Gottesacker" w mieście Herrnhut (Górne Łużyce, Saksonia) to cmentarz istniejący od ponad 300 lat. Lokalne zbiorowiska grzybów intensywnie od lat 60. XX wieku badał G. Zschieschang. Łącząc jego obserwacje z obserwacjami innych mykologów, możemy analizować dane mykologiczne obejmujące okres około 55 lat. Różnorodność biologiczną grzybów oceniamy ze szczególnym uwzględnieniem gatunków CHEGD (*Clavariaceae-Hygrocybe-Entoloma-Geoglossaceae-Dermoloma*). Te gatunki stosowane są w dokumentacji do celów klasyfikacji i oceny, czy użytki zielone zachowują swoją wartość. Na podstawie określonego przez nas profilu CHEGD, „Gottesacker" można zaliczyć do użytków zielonych o znaczeniu międzynarodowym. Ponadto przedstawiamy makroskopowe i mikroskopowe cechy dwóch rzadkich gatunków CHEGD: *Entoloma brunneosericeum* i *Clavaria messapica*. Gatunki te po raz pierwszy zaobserwowano w Saksonii (pierwszy z nich nawet w skali całych Niemiec).

SELF-EXCITED VIBRATION OF INK ROLLERS

Martin Pustka[1]; **Pavel Šidlof**[2]
VÚTS, a.s., Measurement Department,
Svárovská 619, Liberec XI – Růžodol I, 460 01 Liberec, Czech Republic
e-mail: [1]martin.pustka@vuts.cz; [2]pavel.sidlof@vuts.cz

Abstract

A vibration having a character of self-excited chatter oscillation known from machine tools is observed during intermittent motion of ink rollers of offset printing machines. This vibration occurs under specific operating conditions and is often accompanied by an increased noise level. To explain this unusual vibration behavior, a simple analytical model of two rollers interaction is derived. The calculated oscillation is compared with the measurement of ductor roller displacement. The model results confirm the possibility of self-excited vibration development in the presence of viscous forces, negative damping effects and continuous supply of external energy from roller rotation.

Keywords

Self-excited oscillation; Viscous friction force; Negative damping; Offset printing machine.

Introduction

Offset printing is widely used and currently the most important printing technology. The continuous development and automation of offset printing machines provide increased productivity and higher media quality. However, the requirements for higher production speed also increase the dynamic loading of mechanisms, often accompanied by a significant noise and a vibration emission.

The inking unit of offset printing machine transfers the ink from the ink fountain to the plate cylinder [1]. To have a thin, uniform film of ink, the inking unit is composed of a system of many (ten or more) rollers. The quantity of ink supplied to the inking process is determined by the adjustment and the speed of the input part shown in Fig. 1.
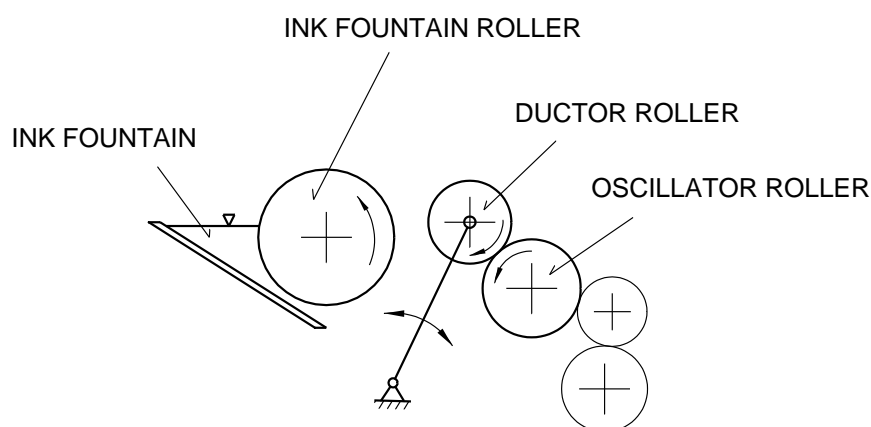
Source: Own
Fig. 1:   *Scheme of the input part of inking unit*

The ink fountain roller and the oscillator roller (including ductor roller tipping mechanism) are driven independently and the rollers have substantially different circumferential velocities. The ductor roller rotates freely and is alternately in contact with the fountain roller and with the oscillator roller to transfer a specified amount of ink. At the moment of contact, the ductor roller abruptly changes its rotational speed.

At high production speeds, the roller impacts are associated with an increased noise and a vibration of the ductor roller. These effects occur only under specific operating conditions, i.e. for rollers covered by an ink layer and at a certain interval of rotational speed. The vibration waveform indicates the potential occurrence of a self-excited oscillation.

1   Research Objectives

The self-induced vibration of ink rollers is an interesting and rather unusual phenomenon. The aim of the research is an initial study of the causes and sources of this vibration behavior including positive and negative damping effects. A simplified analytical model of the roller interaction is created to approximately simulate the measured roller vibration.

2   Vibration of Ductor Roller

An example of a trajectory of ductor axis center point in a plane perpendicular to this axis within one cycle of a reciprocal motion between an ink fountain and an oscillator roller is depicted in Fig. 2. The deflection of the axis center point is derived from the displacement of the ductor surface measured by means of two laser triangulation sensors in the middle of the ductor length. This trajectory is not exactly the same in individual cycles due to a high sensitivity to initial and boundary conditions.
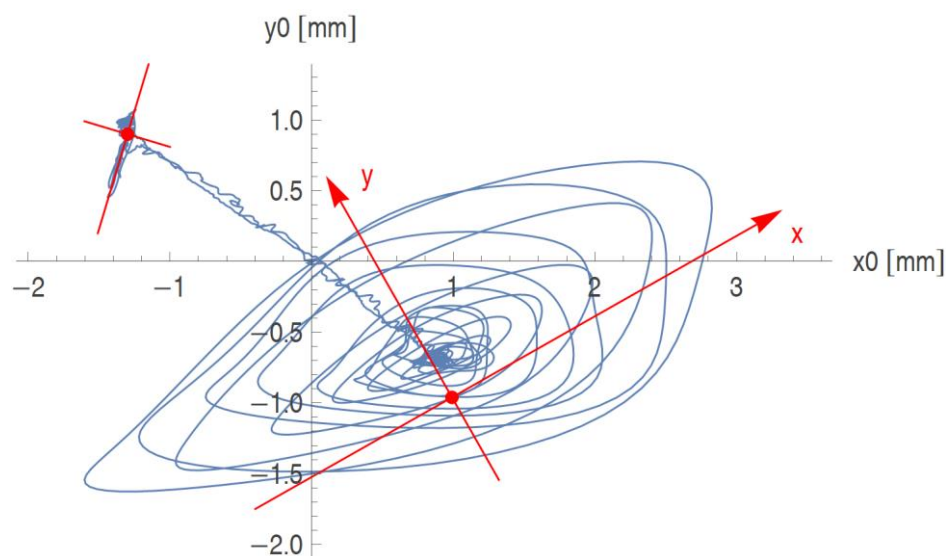
Source: Own

Fig. 2: *Plane motion of ductor axis center point (one cycle of the reciprocal motion between ink fountain and oscillator roller), red – tangent and normal lines to the adjacent rollers at a steady rolling*

An excessive vibration of ductor axis center point (a bending deflection) is clearly seen in both reversal points, particularly at the contact with the oscillator roller. The detail of axis center point displacement (in the direction x of the tangent to the oscillator) and the corresponding sound pressure at the impact on the oscillator are shown in Fig. 3. The measurement microphone was located near the roller surface.
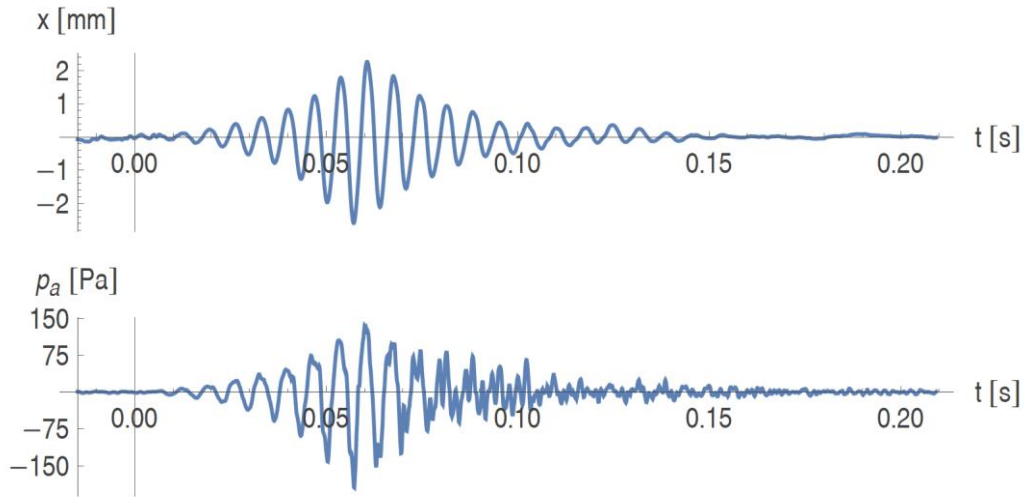
Fig. 3: *The oscillating deflection of ductor axis center point (top) and sound pressure near ductor roller (bottom) at the moment of the impact on the oscillator roller*

The vibration behavior shown in Fig. 3 is apparently non-linear. After the contact of roller ink layers (approximately at a time of 0 s) the vibration amplitudes start to increase gradually with a frequency of ductor fundamental bending mode. This behavior is similar to the self-excited chatter vibrations of machine tools [2] or of other mechanical or fluid systems [3]. The self-excited vibrations are generally characterized by a negative damping, a positive feedback and an energy import from an external source.

After a certain time (approximately at 0.06 s) the vibration amplitudes rapidly reduce, which corresponds to a common characteristic of a damped mechanical system with positive damping. To explain this vibration behavior, a simplified model of the roller interaction is derived in the next chapter.

3 Research Methods

3.1 Model of Roller Vibration

The transient vibration of the ductor roller during the contact of the ductor and the oscillator is modelled using the analytical model depicted in Fig. 4. The model is based on a simplified kinematic geometry of a real system and on a number of other simplifying assumptions. The ductor roller is substituted by a cylindrical disc of mass m and moment of inertia J. The disc axis is flexibly mounted in the horizontal direction x, oscillations in the vertical direction are neglected. The values of stiffness k and viscous damping coefficient b correspond to the eigenfrequency and modal damping of the roller fundamental bending mode [4].

The vertical displacement of the disc is defined by a cam mechanism lift y shown in Fig. 5. In the end position the rollers are compressed and deformed (the ductor has a rubber surface) and the contact area between rollers (a roller nip) is $S = p_0 l$, where p_0 is the static nip width and l is the disc length. Both rollers have the same ink layer of thickness h and at the moment of impact $t = 0$ they are separated by a gap of height $2h$. We suppose that the ink (which is thixotropic in fact) exhibits the Newtonian flow characteristics [5] and has a constant dynamic viscosity η.

Before the impact, the oscillator rotates with a constant angular velocity ω_0 and the angular velocity ω of the disc is zero. At the contact of ink layers (time 0 s in Fig. 5) the viscous

friction force F is developed, which spins the model disc with the increasing velocity ω and simultaneously excites the vibration in the horizontal direction. The force F is proportional to the velocity gradient of ink layer and to the momentary nip width p.
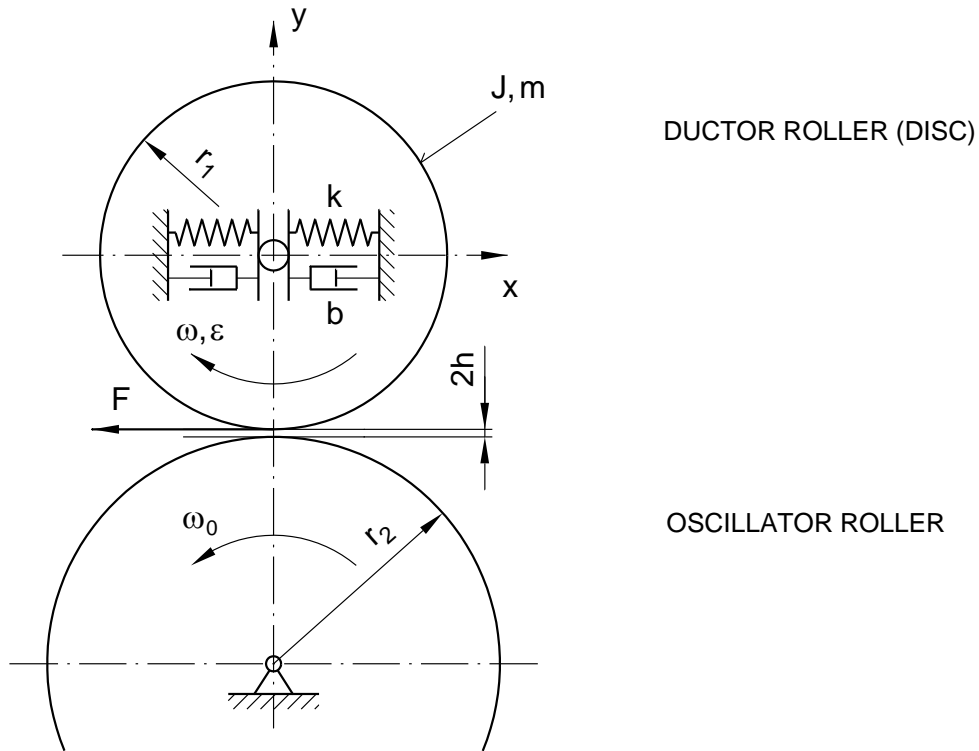
Fig. 4: *Model of ductor roller transient vibration at the roller contact*
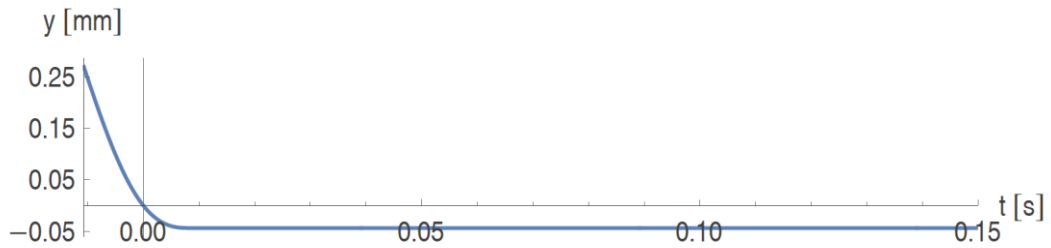
Fig. 5: *Cam lift $y(t)$*

3.2 Equations of Motion

The governing equations of motion have a form

$$m\,\ddot{x}(t) + b\,\dot{x}(t) + k\,x(t) - \frac{J}{r_1}\,\dot{\omega}(t) = 0, \tag{1}$$

$$\frac{J}{r_1}\,\dot{\omega}(t) - \left(r_2\,\omega_0 - r_1\,\omega(t) + b_s(t)\,\dot{x}(t)\right)\frac{1}{2h}\,\eta\,p(t)\,l = 0, \tag{2}$$

where r_1, r_2 are ductor and oscillator diameters. The momentary nip width p satisfies a simplified geometrical condition

$$p(t) = \sqrt{-4\,r_s\,y(t) - y^2(t) - x^2(t)} \text{ for } y(t) < 0 \text{ and } x^2(t) > 4\,r_s\,y(t) + y^2(t), \tag{3}$$

$$p(t) = 0 \text{ elsewhere,} \tag{4}$$

where $r_s = \dfrac{r_1 + r_2}{2}$ is the mean rollers radius.

The variable damping necessary for the self-excited vibration followed by the damped vibration (as discussed in Introduction) is modelled by the damping function b_s, which is introduced into Eq. (2) for the viscous friction force. The function b_s shown in Fig. 6 was created artificially using arctangent function to correspond to the measured time history in Fig. 3.
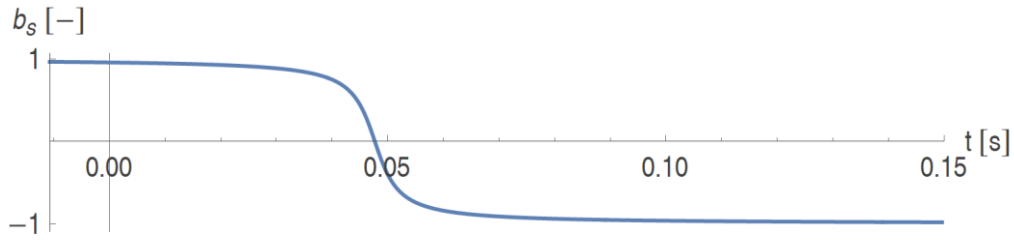
Source: Own

Fig. 6: *Damping function $b_s(t)$*

The model of roller vibration has two degrees of freedom, namely the horizontal displacement of ductor axis x and the ductor angular velocity ω. The resulting time courses can be obtained by a simultaneous solution of Eqs. (1) and (2) with initial conditions $x(0) = 0$ and $\omega(0) = 0$.

4   Calculation Results

The model parameters used for calculation are given in Table 1. These numeric values correspond to the dimensions and parameters of a large-format sheetfed offset press.

Tab. 1: *Calculation parameters*

effective mass m [kg]	8.0
moment of inertia J [kg.m^2]	0.0283
effective stiffness k [N/m]	$6.8 \cdot 10^6$
viscous damping coefficient ($\xi = 3\%$) b [Nms^{-1}]	440
ductor diameter r_1 [m]	0.059
oscillator diameter r_2 [m]	0.076
effective disc length l [m]	0.35
static nip width p_0 [m]	0.003
ink thickness h [m]	10^{-5}
ink viscosity η [Pa.s]	10
oscillator angular velocity ω_0 [rad/s]	78

Source: Own

The calculated time courses of ductor axis displacement x, angular velocity ω, difference velocity Δv and viscous force F are depicted in Fig. 7. The difference of the oscillator and the ductor circumferential velocity Δv is obtained from

$$\Delta v(t) = r_2\omega_0 - r_1\omega(t), \tag{5}$$

the tangential viscous force F between rollers is given by

$$F(t) = \frac{J}{r_1}\,\dot{\omega}(t). \tag{6}$$
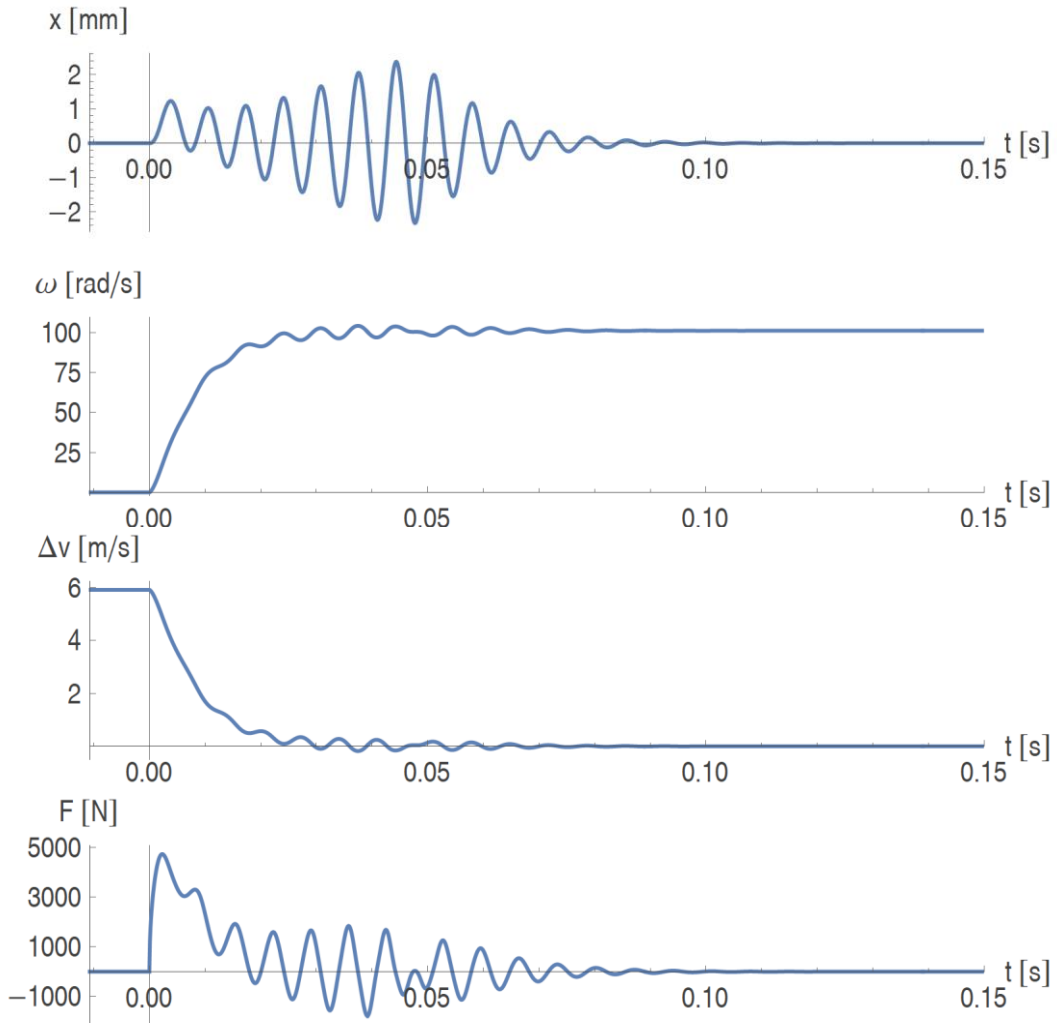
Fig. 7: *Calculated time courses of (top to bottom) ductor disc axis horizontal displacement $x(t)$, angular velocity $\omega(t)$, difference circumferential velocity $\Delta v(t)$ and tangential viscous force $F(t)$*

The time mark at 0 s in Fig. 7 indicates the contact of ink layers (see also Fig. 5). The time course of the axis horizontal displacement x corresponds relatively well to the measured history shown in Fig. 3. The most crucial is the difference of displacement and force amplitudes at the beginning, which is the result of a sudden development of the viscous force F at the rollers contact. The model assumes a constant value of dynamic viscosity η and a constant velocity gradient. However, the local ink viscosity at the contact surface abruptly decreases due to the heating of a small amount of ink caused by friction. With a gradual increase of ductor speed increases also the flow of adhered ink and the ink heating and viscosity decrease are reduced. The force amplitude increases in fact gradually from zero.

The effect of variable damping is clearly visible in Fig. 7. After a stabilization of the angular velocity ω the increasing vibration is suppressed, and the vibration amplitudes rapidly reduce. From this we can conclude that at the beginning the ductor vibration is evidently self-excited with the rotating oscillator roller being an external energy source. When the difference circumferential velocity Δv significantly decreases, the external energy disappears, and the damping of the system becomes positive.

Conclusion

An interesting phenomenon of a vibration similar to a self-excited chatter oscillation was recently observed on printing machines during an intermittent motion of ink rollers. The excessive vibration of ductor roller occurs only in the presence of ink layer at a certain interval of rotational speed and is accompanied by a high noise level.

To clarify the origin of this vibration under quite complicated conditions, a simplified analytical model of rollers contact was created. The model results indicate a probable source of the vibration behavior, which is a viscous friction force originating in the ink layer between rollers. In the presence of an energy import caused by different circumferential velocities of both rollers the ink layer interaction creates a positive feedback, which excites the self-oscillation of the ductor roller. The excitation effect of the viscous force rapidly disappears after the velocity difference significantly decreases.

The simplified model describes this vibration problem only approximately and the process of roller self-excitation should be further analyzed, e.g., by means of advanced modelling using FEM and computational fluid dynamics methods.

Acknowledgements

Literature

[1]   KIPPHAN, H. (ed.): *Handbook of Print Media: Technologies and Production Methods*. Springer-Verlag Berlin Heidelberg, 2001. ISBN 978-3-540-67326-2. eBook ISBN 978-3-540-29900-4. DOI: 10.1007/978-3-540-29900-4

[2]   QUINTANA, G.; CIURANA, J.: Chatter in machining processes: A review. *International Journal of Machine Tools and Manufacture*. 2011, Vol. 51, Issue 5, pp. 363–376. DOI: 10.1016/j.ijmachtools.2011.01.001

[3]   TONDL, A.: To the problem of self-excited vibration suppression. *Engineering Mechanics*. 2008, Vol. 15, Issue 4, pp. 297–307. Available from WWW: http://www.engineeringmechanics.cz/pdf/15_4_297.pdf

[4]   BREPTA, R.; PŮST, L.; TUREK, F.: *Mechanické kmitání*. Sobotáles, Praha, 1994. ISBN-13 978-80-901684-8-0. ISBN 80-901684-8-5.

[5]   CHHABRA, R. P.: Non-Newtonian Fluids: An Introduction. In: Krishnan J.; Deshpande A.; Kumar P. (eds), *Rheology of Complex Fluids*. Springer, New York, NY, 2010, pp. 3–34. ISBN 978-1-4419-6493-9. Online ISBN 978-1-4419-6494-6. DOI: 10.1007/978-1-4419-6494-6_1

doc. Ing. Martin Pustka, Ph.D.; Ing. Pavel Šidlof, CSc.

Samobuzené kmitání barvicích válců

Při střídavém pohybu barvicích válců tiskového stroje se vyskytují vibrace mající charakter samobuzených kmitů, které jsou známy například u obráběcích strojů. Tyto vibrace vznikají při určitých provozních podmínkách a jsou často doprovázeny zvýšenou hladinou hluku. Pro objasnění tohoto neobvyklého kmitavého chování je odvozen jednoduchý analytický model vzájemného působení dvou válců. Vypočtené vibrace jsou porovnány s měřením posunutí barvicího válce. Výsledky modelování potvrzují možnost vyvolání samobuzených kmitů při přítomnosti viskózních sil, účinků záporného tlumení a přívodu vnější energie tvořené otáčením válce.

Selbsterregte Schwingung der Farbwalzen

Bei der intermittierenden Bewegung der Farbwalzen tritt eine Schwingung auf, die den Charakter einer selbsterzeugten Schwingung hat und die aus dem Bereich der Werkzeugmaschinen bekannt ist. Diese Schwingung entsteht unter bestimmten Betriebsbedingungen und wird oft von Geräuschemission begleitet. Für die Erklärung dieses ungewöhnlichen Schwingverhaltens wird das einfache analytische Modell der Zwei-Walzen-Gegenwirkung entworfen. Die berechnete Schwingung wird mit der Messung des Wegs von Farbwalzen verglichen. Die Modellergebnisse bestätigen die Möglichkeit, eine selbsterzeugte Schwingung in Gegenwart von Viskoskräften, von Wirkungen negativer Dämpfung und der Zuführung der äußeren Energie der Walzendrehung zu erzeugen.

Drgania samowzbudne wałków farbowych

Podczas przemiennego ruchu wałków farbowych maszyny drukarskiej występują drgania mające charakter drgań samowzbudnych, które występują przykładowo w maszynach do obróbki. Drgania te powstają w pewnych warunkach eksploatacyjnych i często towarzyszy im wyższy poziom hałasu. Dla wyjaśnienia tych nietypowych drgań opracowano prosty model analityczny wzajemnego oddziaływania dwóch wałków. Obliczone drgania porównano z pomiarami przesunięć wałka farbowego. Wyniki modelowania potwierdzają możliwość wywołania drgań samowzbudnych w obecności oporu wiskotycznego, oddziaływania oporu ujemnego i wpływu energii zewnętrznej generowanej przez obroty wałka.

LIST OF AUTHORS

Name	E-Mail and Page Number of Contribution	
Wolfgang Förster	wolfgang.foerster@ba-sachsen.de	7
Thomas Pucklitzsch	thomas.pucklitzsch@ba-sachsen.de	7
Daniela Nickel	daniela.nickel@ba-sachsen.de	7
Alexander Karich	alexander.karich@tu-dresden.de	17
René Ullrich	rene.ullrich@tu-dresden.de	17
Martin Hofrichter	martin.hofrichter@tu-dresden.de	17
Martin Pustka	martin.pustka@vuts.cz	29
Pavel Šidlof	pavel.sidlof@vuts.cz	29

GUIDELINES FOR CONTRIBUTORS

Guidelines for contributors are written in the form of a template which is available as a Word document at http://acc-ern.tul.cz/images/journal/ACC_Journal_Template.docx.

Upozornění pro čtenáře

Příspěvky v časopise jsou recenzovány a prošly jazykovou redakcí.

Readers' notice

Contributions in the journal have been reviewed and edited.

Předplatné

Objednávky předplatného přijímá redakce. Cena předplatného za rok je 900,- Kč mimo balné a poštovné. Starší čísla lze objednat do vyčerpání zásob (cena 200,- Kč za kus).

Subscription

Subscription orders must be sent to the editorial office. The price is 40 € a year excluding postage and packaging. It is possible to order older issues only until present supplies are exhausted (8 € an issue).

Časopis ACC JOURNAL vychází třikrát ročně (červen, září, prosinec).
Three issues of ACC JOURNAL are published every year (June, September, December).